Comunicata Scientiae
Horticultural Journal

ORIGINAL ARTICLE
published: 31 December 2021
https://doi.org/10.14295/CS.v12.3593

Three-dimensional numerical simulation of the thermal and aerodynamic behavior of a roof structure built on a slope and used for horticultural production

Edwin Andres Villagran Munar*, Carlos Ricardo Bojaca Aldana

Universidad de Bogota Jorge Tadeo Lozano, Bogotá, Colombia
*Corresponding author, e-mail: eavillagranm@unal.edu.co

Abstract

In tropical countries, part of the horticultural production is carried out in hillside soils. In recent years, due to the adverse effects of climate change and other biotic factors that limit and affect agricultural production, the use of roof structures has been promoted as a technological means to improve production in this type of production system. The microclimate study of structures built on slopes is scarce, therefore farmers continue to build the same type of structure without technical design criteria and without knowing if the microclimate conditions generated are suitable for the crops. In the present research work, an experimentally validated 3D CFD numerical model was implemented to analyze air flows and spatial temperature behavior in a roof structure built on a site with broken topography. The results obtained allowed us to find out that the air flows are strongly affected by the longitudinal and transversal slopes of the land, which produces low ventilation rates that generate thermal gradients above 8 °C and highly heterogeneous thermal behavior, factors that are not suitable for horticultural production.

Keywords: CFD simulation, Airflow, Temperature

Introduction

In Colombia the horticultural production is concentrated mainly in the Andean region, this region presents a high diversity of geographical and climatic conditions that allows the production of a great variety of vegetable products during the different seasons of the year. This region has approximately 14 million hectares with soils suitable for agriculture, a high percentage of which is found in broken terrain with moderate slopes (Rodríguez-Leyton, 2019).

In recent years, in the search to increase the profitability and yields of these production systems and as an alternative for adaptation to the adverse effects of climate change, farmers have started to implement roof structures built on land with longitudinal and transversal slopes (Villagrán et al., 2020). It should be noted that at the local and regional level the study of the microclimate in this type of construction is quite scarce since most of the roof structures or greenhouses were always built on flat land or in plateau regions (Reynafarje et al., 2020).

The type of structures used by the farmers are built according to the producer's criteria and with a low technological level, factors that make them accessible to many end-users. Although on many occasions these producers do not consider and even ignore the behavior of the microclimate generated inside these structures. Therefore, this information needs to be generated since the microclimate is a factor that directly affects agricultural production in roof structures (Taki et al., 2016). One of the most used methodologies for the study of the microclimate in agricultural buildings is computational fluid dynamics, which is a robust technique that allows obtaining specific results in moderate periods (Villagrán et al., 2019).

The objective of this research was to implement and validate a three-dimensional numerical simulation

Received: 10 September 2020
Accepted: 21 June 2021

model, to be used as a tool to evaluate the airflow patterns and the spatial distribution of temperature inside a traditional Colombian roof structure built on a hillside, the numerical simulations considered the dominant climatic conditions of the study region.

Materials and methods

Climatic conditions and description of the structure

The experimental study was carried out in the town of Filandia (75°40´50.3" W, 4°42´12.3" N and altitude: 1476 m) in the department of Quindío in Colombia. The multiannual behavior on a monthly scale of the main agroclimatic variables is summarized in Figure 1. The average temperature value shows a value of 20.95 °C with maximum and minimum values of 26.6 °C and 15.4 °C respectively, while the accumulated annual precipitation shows a value of 2060 mm.

The behavior of the wind is quite variable both in its speed and direction component it can be identified that the percentages of wind coming from each of the four cardinal points are redistributed each month of the year, where the percentage of direction more dominant is the wind coming from the south (Figure 1). Likewise, the speeds of these events, which were grouped into three-speed intervals: low speed [0 m s^{-1} - 0.3 m s^{-1}], medium-low speed [0.3 m s^{-1} - 1.1 ms^{-1}], and medium-high speed [1.1 m s^{-1} - 2.0 ms^{-1}], show that for 7 of the 12 months of the year the low speeds dominate and for the remaining 5 months the medium-high speed dominates (Figure 1).

For the validation and later application of the CFD model, experimental measurements were carried out on a traditional Colombian naturally ventilated roof structure (TSA). The area of soil under the roof was 2040 m^2 corresponding to a longitudinal (W-E) and transversal (N-S) dimension of 50 m and 40.8 m respectively (Figure 2). The TSA structure is built in a zone of broken topography that presents a longitudinal (S_L) and transversal (S_C) slope of 51 % and 22.5 % respectively.

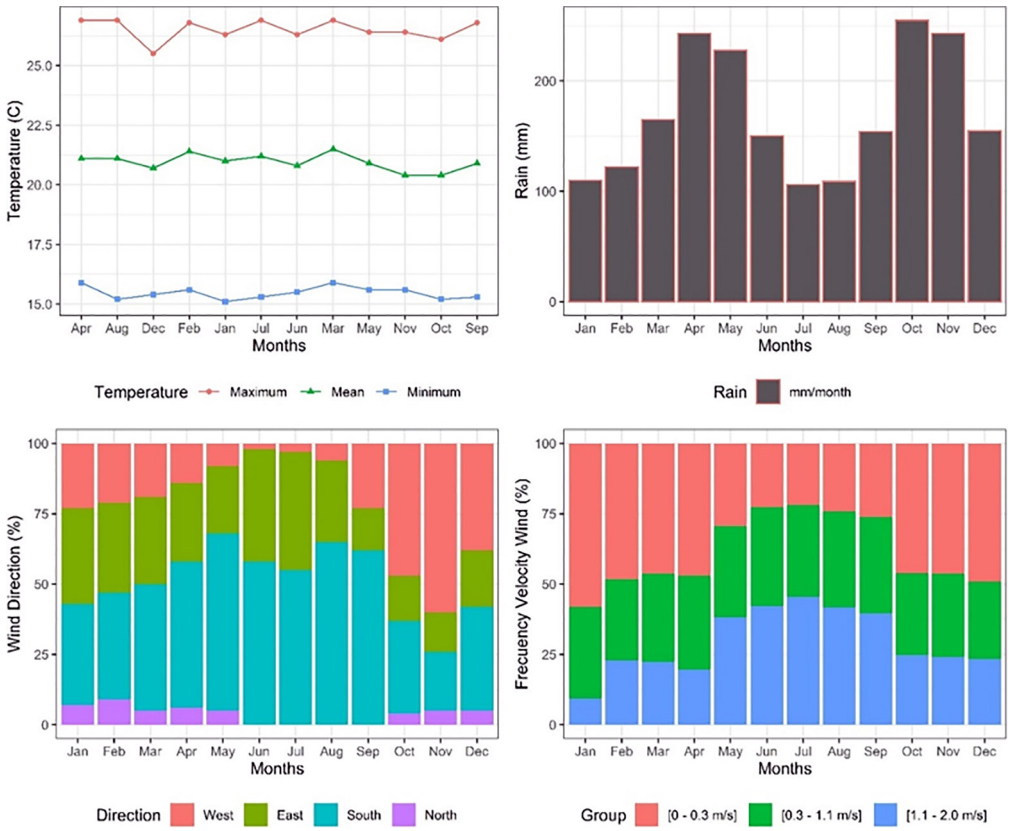

Figure 1. Multi-annual behavior of the main agro-climatic variables.

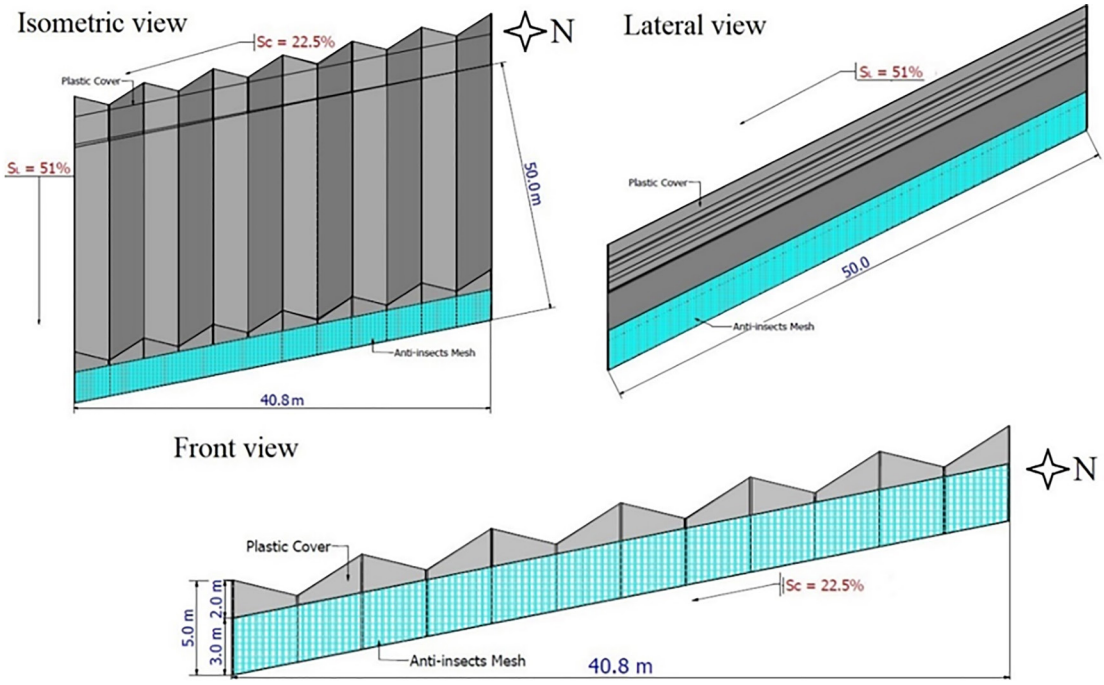

Figure 2. General dimensions of the evaluated structure.

The minimum and maximum height of the structure is 3.5 m and 5.0 m respectively, the TSA roof is made of steel cables and a commercial polyethylene film, the structure only has ventilation areas on the sidewalls and facades, regions that are covered with an insect-proof screen with a wire density (threads cm^{-1}× threads cm^{-1}) of 16.1 × 10.2.

CFD simulation

The CFD methodology allows the calculation of airflow patterns and heat distribution patterns generated inside a protected agricultural structure, the numerical CFD simulation is divided into 3 main stages, pre-process, solution, and post-process. In the pre-process the physical problem to be solved is defined, the virtual model of the geometry of the structure object of study is generated, the size of the computational domain is defined and the size of the numerical mesh for the whole computational domain. In the solution, the numerical models are selected for simulation, the boundary and convergence conditions are defined, and the initial simulation conditions are established. Finally, in the post-process, the exploration and obtaining of qualitative and quantitative data necessary to validate the CFD model and to carry out the analysis corresponding to the objective of the investigation is carried out.

For this pre-processing phase, a computational domain was established that had a size of 240.8 m, 50 m, and 250 m for the x, y, and z axes respectively, this size was defined about the maximum height of TSA (H = 5 m), therefore the perimeter edges were defined at a distance of 20 H and the upper edge at a minimum distance of 10H, as recommended by several numerical studies of natural ventilation of buildings (Perén et al., 2016). To determine the size of the numerical grid to guarantee solution independence at this size, adequate convergence, and acceptable computational performance, a total of 8 numerical grids were evaluated with different element sizes in the range [950,876 – 28,345,679]. The selected grid was number 4 which contains a total of 16,675,918 square elements conformed in an unstructured grid (Figure 3B, C). The grid independence test was performed according to the one developed by Villagrán et al. (2019), while the quality of the grid was evaluated using the orthogonality criterion for which 94.2 % of the cells were in the high-quality range (Román-Roldán et al., 2019; Toghraie et al., 2018).

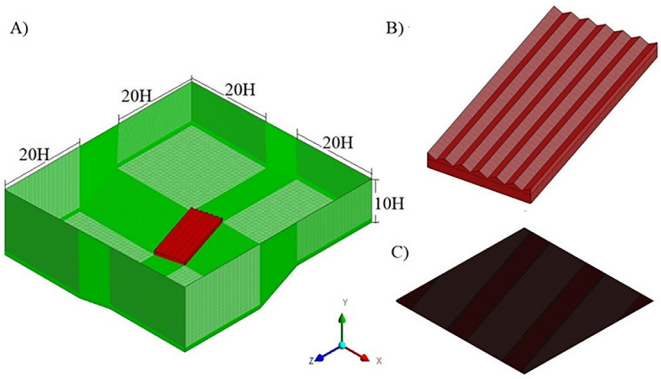

Figure 3. A) Computational domain and B) Numerical grid of the structure and C) Detail of the grid.

The numerical solution is developed from the spatial discretization of the non-linear partial equations of Navier-Stokes. The transport phenomena via free convection can be described by equation (1) which is considered the general transport equation for a steady-state fluid in a three-dimensional field of action.

$$\frac{\partial(u_{\emptyset})}{\partial x}+\frac{\partial(v_{\emptyset})}{\partial y}+\frac{\partial(w_{\emptyset})}{\partial z}=\Gamma\nabla^2\emptyset+S_{\emptyset} \quad (1)$$

Where y, x, and z are the coordinates in Cartesian space, u, v, and w represent the components of the velocity vector, ∇^2 is the Laplacian operator, Γ is the diffusion coefficient, $\emptyset$ is the concentration of the quantity transported in a dimensional form and $S_{\emptyset}$ is the source term. Reynolds' stress tensor was applied to the numerical model through the use of the empirical model *k* - ε standard, model that has been widely validated in studies of natural ventilation of agricultural buildings, showing a great adjustment of the real behavior of the airflow concerning the simulated process (Piscia et al., 2015).

Also, the effect of air buoyancy caused by the force of gravity and air density changes were added to the momentum equation as a source term by Boussinesq's approximation (Aich et al., 2018). The presence of insect-proof screens in the ventilation areas of the structure was modeled with a porous medium approach, considering their non-linear moment loss coefficient and their permeability as a function of screen porosity. The aerodynamic coefficients requested by the CFD model were established for the type of insect screen used which is similar to that reported in the study developed by Villagrán et al. (2020). The radiation model selected was the discrete ordinate (DO) model with angular discretization, this model allows calculating the radiation and convective exchanges that occur in the computational domain, treating the greenhouse roof as a semi-transparent medium (Baxevanou et al., 2018).

The boundary conditions established to the computational domain were of symmetrical properties for the sides parallel to the air flow direction, the air flow output limit was established as a pressure output limit. For the air inlet limit, a speed inlet condition was established with a logarithmic profile establishing the soil roughness parameters according to the conditions of the study site and applying to the numerical model the shape with is explained in the study of King et al. (2017). For the cover areas of the structure and the floor of the computational domain, wall conditions were established while for the areas where the insect-proof porous screen has established a limit of the porous medium, in each one of these regions the optical and physical properties of each one of the materials were defined and are summarized in Table 1.

Table 1. Properties of materials used in the CFD simulation.

Physical and optical properties of the materials				
	Ground	Air	porous screen	Polyethylene
Density (ρ, kg m^{-3})	1.300	1.225	960	950
Thermal conductivity (k, W m^{-1} K^{-1})	1.3	0.0242	0.45	0.4
Specific heat (Cp, J K^{-1} kg^{-1})	1.718	1,006.43	1.870	2450
Coefficient of thermal expansion (K^{-1})		0.0033		
Absorptivity	0.89	0.19	0.26	0.07
Scattering coefficient	-10	0	0	0
Refractive index	3	1	0.09	1.65
Emissivity	0.91	0.9	0.60	0.8

Validation of the CFD model and simulated scenarios

The generated CFD model was validated by experimental tests inside the TSA structure. This experimental phase was carried out during the period from April 6, 2019, to October 9, 2019, and involved the recording and subsequent storage of the main climatic variables in the external environment of the structure, with a measurement frequency of 10 minutes.

Also, inside the structure on the longitudinal middle region (z axis=25 m) and on a cross-section of the structure and a height of 1.6 m above the ground, 10 temperature recording sensors and 3 sonic anemometers for recording wind speed were placed, which recorded data every 10 minutes during the experimental phase. The climate information captured in the experimental period was analyzed and 3 hours of the day were selected to perform the validation simulations. In these simulations, the values of the variables reported in Table 2 were used.

Table 2. Mean climatic conditions by hour obtained for the experimental period.

Hour	Temperature (°C)	Solar radiation (W m^{-2})	Wind speed (m s^{-1})	Wind direction
07	20.8	54	0.4	S
11	23.8	543	1.1	S
14	26.1	705	1.6	S

To evaluate the validity of the numerical model, once the hourly simulations were completed, temperature and air velocity data were extracted for each sampling point inside TSA. These simulated data were compared with the data measured through the goodness-of-fit parameters as mean absolute error MAE equation (2), root mean square error (RMSE) equation (3).

$$MAE = \frac{1}{M}\sum_{j=1}^{N}|Dxmj - Dxsj| \quad (2)$$

$$RMSE = \sqrt{\sum_{j=1}^{M}\frac{|Dxm_i - Dxs_i|^2}{M}} \quad (3)$$

Where $\overline{Tm}$ is the average of the measured values, Dxm_j, Dxs_j are the measured and simulated wind speed and temperature values at a point j respectively and *N* is the number of samples.

Once the validity of the numerical model was checked, it was used for this research work for which 12 simulations were developed with the initial conditions established in the scenarios in Table 3. These conditions are equivalent to the conditions of maximum radiation and environment temperature and 3 levels of wind speed for the 4 cardinal points which are characteristic conditions of the region of study (Figure 1).

Table 3. Simulation initial conditions for each evaluated scenario.

Hour	Temperature (°C)	Solar radiation (W/m²)	Wind speed (m/s)	Wind direction
E1V1	26.8	763	0.3	N
E1V2	26.8	763	1.1	N
E1V3	26.8	763	2.0	N
E2V1	26.8	763	0.3	S
E2V2	26.8	763	1.1	S
E2V3	26.8	763	2.0	S
E3V1	26.8	763	0.3	W
E3V2	26.8	763	1.1	W
E3V3	26.8	763	2.0	W
E4V1	26.8	763	0.3	E
E4V2	26.8	763	1.1	E
E4V3	26.8	763	2.0	E

Results and Discussion

Model validation

The qualitative results of the validation process are summarized in Figure 4. In general, for the temperature, the graphs of the simulated data show behavior and trend like those obtained experimentally. Likewise, for the wind speed variable, it is observed that the experimental data present a value close to those obtained in the numerical simulation. The MAE values were 0.23 °C, 0.27 °C and 0.30 °C and 0.01 m s^{-1}, 0.03 m s^{-1} and 0.04 m s^{-1} for hours 07, 11 and 14 respectively, while the RMSE values were 0.27 °C, 0.33 °C and 0.31 °C and 0.01 m s^{-1}, 0.03 m s^{-1} and 0.05 m s^{-1} for the same hours.

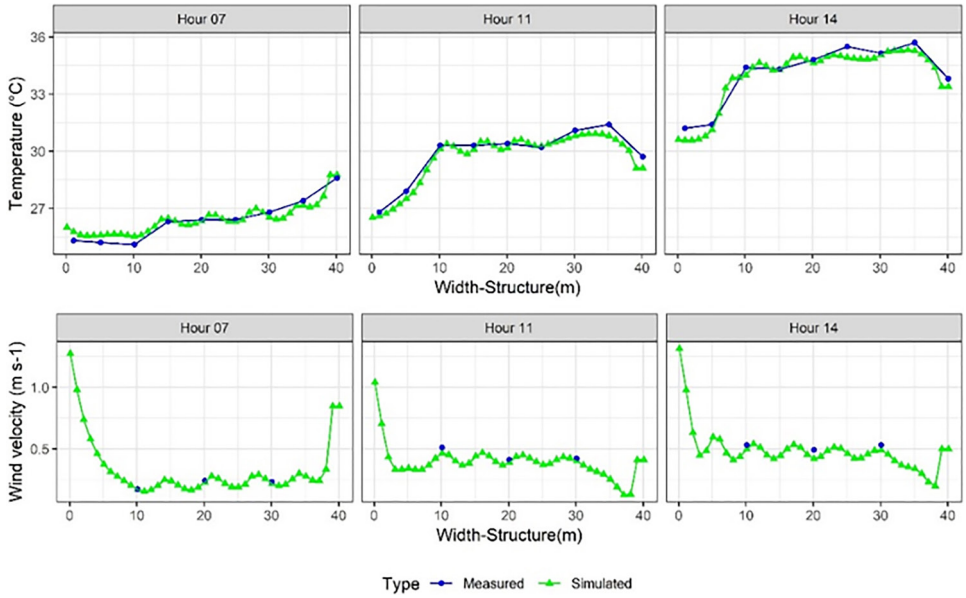

Figure 4. Temperature and wind speed trends measured and simulated.

These values are within the range reported in studies with a similar focus as that developed by Villagrán et al. (2019), therefore the model can be considered to have a high capacity to predict the temperature and airflow behavior inside TSA.

Airflow behavior and ventilation rates

The airflow patterns generated inside the TSA structure are shown in Figure 5. For E1V1, E1V2, and E1V3 a behavior is observed where the airflow enters from the windward side, and once inside the TSA, these flows are directed towards the upper façade and the upper third of the leeward side, regions where the airflow leaves the structure. It can also be seen that there is an airflow near the lower facade of TSA that enters from the windward side and is directed horizontally towards the leeward side. This differentiated flow may be caused by the low impact of the longitudinal slope on this area of the structure (Figure 5). Also in this area, there is a flow of air with greater intensity and speed, this is a consequence of the strong interaction that exists in this region between the porous mesh and the outside environment (Teitel et al., 2011; Villagrán et al., 2020).

These behaviors analyzed above are repeated for scenarios E2V1, E2V2, and E2V3, although in the opposite direction since for these scenarios the wind comes from the cardinal point opposite to that of scenario E1. This allows us to conclude that for structures built on land with broken topography the slope has a strong incidence on the flow patterns developed inside these structures.

In the case of the E3V1 scenario, air flows enter the structure through the upper and lower facades and the left side section, air flows that seek to exit TSA through the right-side wall. On the other hand, for the E3V2 and E3V2 scenarios, airflow is observed that enter TSA through the lower facade and the left side wall, these air flows inside TSA move in the opposite direction to the exterior airflow and is directed towards the highest regions in both the longitudinal and transversal directions, and it is precisely over these regions that TSA exits (Figure 5).

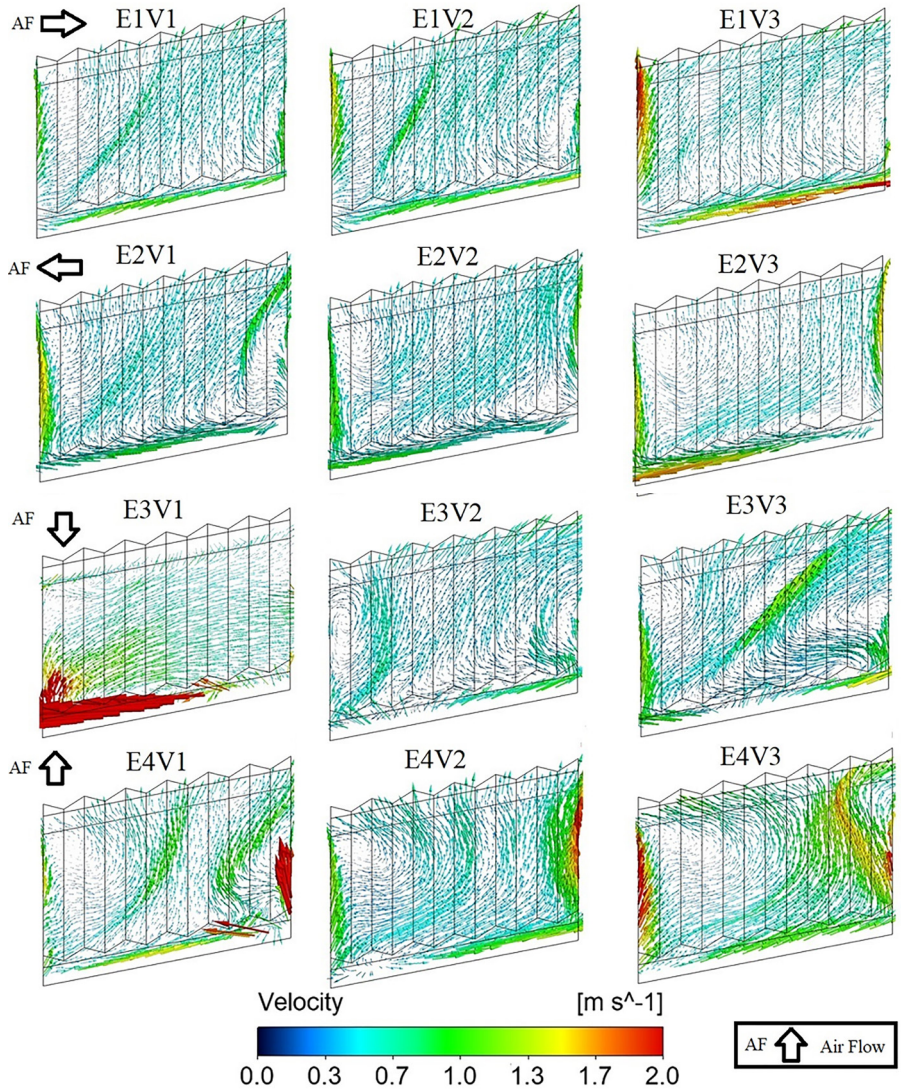

Figure 5. Simulated airflow patterns for each scenario evaluated.

Finally, for scenarios E4V1, E4V2, and E4V3, air flows are observed entering TSA through the lower façade and the left side wall, air flows that are accelerated from the central region of TSA towards the left side moving in a longitudinal direction towards the highest area of the structure, until exiting TSA through the façade and the upper third of the right sidewall.

To determine the quantitative behavior of the airflow, the simulated air velocity data were extracted from the TSA for each scenario, and the mean velocity and the normalized velocity, which is equivalent to the relationship between the inside air velocity and the outside air velocity, were calculated from the data sets (Table 4). In general terms, the mean airflow velocity oscillates between a minimum value of 0.27 ± 0.13 m s^{-1} in the case of E1V1 and a maximum value of 0.70 ± 0.32 m s^{-1} for E3V3. Values that are lower than those reported by López et al. (2016) in an experimental study of natural ventilation in a greenhouse located on flat terrain and equipped with anti-insect screens on the side and roof vents.

On the other hand, for the normalized velocity, it is possible to observe that for the lower velocity scenarios V1 is where the lowest reductions in airflow velocity within TSA occur 9.9 % and 23.4 % for E1 and E2 respectively. While for E3 and E4 there are conditions of higher mean normalized velocity, in these scenarios this may be influenced because, under conditions of low outdoor wind speed, the air flows in TSA will be dominated by the thermal effect of natural ventilation and in turn, there may be an acceleration of flow caused by the slopes of the terrain.

In the case of the scenarios of medium speed V2 and high-speed V3, it can be seen that the flow reductions are greater as the speed of the outside wind increases, although this speed reduction is more critical for E1 and E2 with values between 73.8 % and 75.9 %, results that are in agreement with what was reported in the study developed by Flores-Velazquez and Montero (2008), in a screen house and who adjusted a linear regression line to this type of behavior.

Table 4. Airflow assessment parameters for each simulation scenario.

Scenario	Mean velocity (ms-1)	Normalized velocity (%)	Scenario	Mean velocity (ms-1)	Normalized velocity (%)
E1V1	0.27 ± 0.13	90.1 ± 43.3	E3V1	0.39 ± 0.25	130.1 ± 83.3
E1V2	0.43 ± 0.16	39.1 ± 14.7	E3V2	0.42 ± 0.11	38.2 ± 10.0
E1V3	0.52 ± 0.23	26.2 ± 11.5	E3V3	0.50 ± 0.24	25.2 ± 12.0
E2V1	0.23 ± 0.16	76.6 ± 53.3	E4V1	0.38 ± 0.24	126.6 ± 80.1
E2V2	0.42 ± 0.14	38.2 ± 12.7	E4V2	0.53 ± 0.21	48.2 ± 19.1
E2V3	0.48 ± 0.21	24.1 ± 10.5	E4V3	0.70 ± 0.32	35.1 ± 16.2

The behavior of the ventilation rates (Φ) calculated for each scenario is shown in Figure 6. It can be observed that there is a linear behavior between the value of Φ and the speed of the outside wind, therefore, the higher the velocity of Φ, this has been demonstrated in several studies of natural ventilation in passive greenhouses such as the one developed by Baeza et al. (2009). On the other hand, it should also be mentioned that the values of Φ for all scenarios varied between a minimum of 0.003 $m^3 s^{-1} m^{-2}$ for E1V1 and a maximum of 0.012 $m^3 s^{-1} m^{-2}$ for E4V3.

These values of Φ are very far below the minimum recommended value for ventilated greenhouses of course which is Φ =0.04 $m^3 s^{-1} m^{-2}$ (Baeza et al., 2009; Villagrán et al. 2020),a value that can guarantee an adequate microclimate behavior of the evaluated structure (Khaoua et al., 2006). These low ventilation rate values may be influenced by the presence of anti-insect mesh in the TSA ventilation areas and more specifically by the loss of impulse generated in the air flows caused by the presence of this low-porosity material (Flores-Velazquez et al., 2013). Another factor that may be the cause of the low values of Φ, is the unavailability of ventilation areas in the roof area of TSA, ventilation areas that would allow maximizing the exchange of air via free convection or air buoyancy.

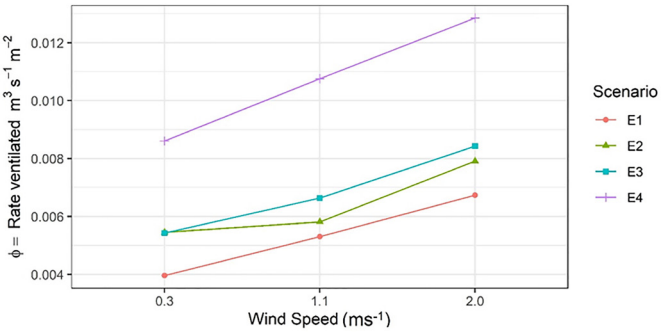

Figure 6. Ventilation rates calculated for each scenario evaluated.

Spatial distribution of temperature

The spatial temperature distributions inside the TSA for each scenario are shown in Figure 7. In general terms, there is a very similar pattern of thermal distribution

in each scenario evaluated, where the lower temperature areas are presented near the lower facade. Likewise, the highest temperature zones are located from the central zone of the structure to the upper façade and in some cases, such as in E1V2, E2V1, E3V2, E3V4, the high-temperature regions are located above the region with the highest height above the terrain and just where the air flows out of the greenhouse.

These temperature distribution patterns differ from those reported in other studies where the hottest areas are located in the leeward region and the coldest areas in the windward region (Villagrán Munar & Bojacá Aldana, 2019), as mentioned above may be influenced by the slopes of the land where the structure was built. It is also easy to identify qualitatively that there is high heterogeneity in the spatial distribution of the temperature inside TSA and thermal gradients that easily exceed 8 °C in a high percentage of the scenarios evaluated, such behavior is characteristic of passive structures with poor ventilation rates (Espinoza et al., 2017; McCartney et al., 2018).

For the quantitative analysis of this variable, the mean values of the temperature inside the structure and the mean thermal differential were determined ($\Delta T_{m=}$ Tinside- Toutside) for each of the scenarios analyzed (Table 5). The temperature values ranged from a minimum of 34.3 ± 2.67 °C for E2V3 to a maximum of 39.5 ± 2.43 °C for E4V, it should also be mentioned that the temperature values exceed or are very close to 35 °C recommended value to ensure adequate growth and development of a high percentage of plants grown under protected agricultural systems (Saberian & Sajadiye, 2019).

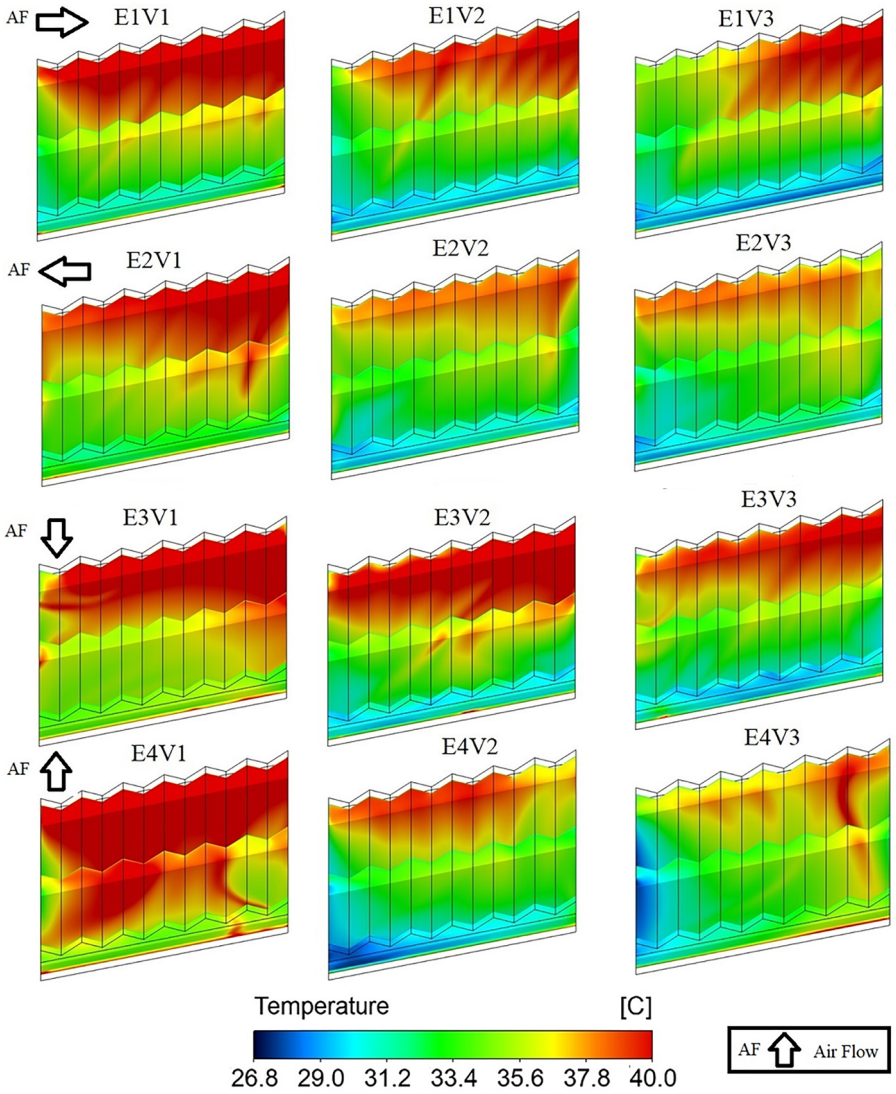

Figure 7. Simulated thermal distribution patterns for each scenario evaluated.

The values of standard deviation allow to demonstrate that a high heterogeneity exists in the behavior of the temperature, this factor affects the growth and development of the cultures when modifying spatially the physiological phenomena like the transpiration and the absorption of nutrients of the plants, set of plants that are managed culturally of homogenous form for labors like; irrigation and fertilization in this type of structure (Taki et al., 2016; Villagrán and Bojacá, 2020). Lastly, the values of ΔTm ranged from 7.6 ± 2.67 °C to 12.2 ± 2.43 °C, values that are higher than those of Senhaji et al. (2019), in a greenhouse studio equipped with insect-proof screens.

Table 5. Thermal parameters evaluated for each simulation scenario.

Scenario	Mean Temperature (°C)	ΔT_m (°C)	Scenario	Mean Temperature (°C)	ΔT_m (°C)
E1V1	36.5 ± 2.91	9.7 ± 2.91	E3V1	37.1 ± 2.81	10.3 ± 2.81
E1V2	35.0 ± 2.85	8.2 ± 2.85	E3V2	36.4 ± 3.09	9.6 ± 3.09
E1V3	34.8 ± 2.70	7.9 ± 2.70	E3V3	34.9 ± 2.92	8.1 ± 2.92
E2V1	36.6 ± 3.07	9.8 ± 3.07	E4V1	39.5 ± 2.43	12.2 ± 2.43
E2V2	34.6 ± 2.74	7.8 ± 2.74	E4V2	34.5 ± 3.05	7.75 ± 3.05
E2V3	34.3 ± 2.67	7.6 ± 2.67	E4V3	34.6 ± 2.54	7.81 ± 2.54

Conclusions

Flow patterns generated inside the evaluated structure are strongly affected by the topography of the terrain and by the unavailability of ventilation areas in the roof region of the structure, resulting in inadequate ventilation rates well below the minimum recommended value for naturally ventilated roof structures.

Deficiencies in ventilation of the evaluated structure generate highly heterogeneous thermal behavior with thermal gradients between 7.6 ± 2.67 °C and 12.2 ± 2.43 °C.

Future work may use the numerical model validated in this research to design a structure that optimizes air flows, maximizing ventilation rates, and improving thermal behavior about current structures used in hillside areas.

References

Aich, W., Kolsi, L., Borjini, M.N., Al-Rashed, A.A., Aissia, H. B., Oztop, H.F., Abu-Hamdeh, N. 2018. Three-dimensional computational fluid dynamics analysis of buoyancy-driven natural ventilation and entropy generation in a prismatic greenhouse. *thermal science* 22: 73-85.

Baeza, E.J., Pérez-Parra, J.J., López, J.C., Gázquez, J.C., Kacira, M., Montero, J. I. 2009. Validation of CFD simulations for three dimensional temperature distributions of a naturally ventilated multispan greenhouse obtained by wind tunnel measurements. *Acta Horticulturae 893*: 571-579.

Bartzanas, T., Boulard, T., Kittas, C. 2002. Numerical simulation of the airflow and temperature distribution in a tunnel greenhouse equipped with insect-proof screen in the openings. *Computers and electronics in agriculture* 34: 207-221.

Baxevanou, C., Fidaros, D., Bartzanas, T., Kittas, C. 2018. Yearly numerical evaluation of greenhouse cover materials. *Computers and Electronics in Agriculture* 149: 54-70.

Espinoza, K., López, A., Valera, D.L., Molina-Aiz, F.D., Torres, J.A., Pena, A. 2017. Effects of ventilator configuration on the flow pattern of a naturally-ventilated three-span Mediterranean greenhouse. *Biosystems Engineering*164: 13-30.

Flores-velazquez, J., Guerrero, F.V., Lopez, I.L., Montero, J.I., Piscia, D. 2013. 3-Dimensional thermal analysis of a screenhouse with plane and multispan roof by using Computational Fluid Dynamics (CFD). *Acta Horticulturae* 1008: 151-158.

Flores-velazquez, J., Montero, J.I. 2008. Computational Fluid Dynamics (CFD) study of large scale screenhouses. *Acta Horticulturae* 797:117-122.

Flores-velazquez, J., Ojeda, W., Villarreal-Guerrero, F., Rojano, A. 2015. Effect of crops on natural ventilation in a screenhouse evaluated by CFD simulations. *Acta Horticulturae* 1170: 102.

King, M.F., Gough, H.L., Halios, C., Barlow, J. F., Robertson, A., Hoxey, R., Noakes, C. J. 2017. Investigating the influence of neighbouring structures on natural ventilation potential of a full-scale cubical building using time-dependent CFD. *Journal of Wind Engineering and Industrial Aerodynamics169*: 265-279.

López, A., Molina-Aiz, F.D., Valera, D.L., Peña, A. 2016. Wind tunnel analysis of the airflow through insect-proof screens and comparison of their effect when installed in a Mediterranean greenhouse. *Sensors 16*: 690-671.

Mccartney, L., Orsat, V., Lefsrud, M.G. 2018. An experimental study of the cooling performance and airflow patterns in a model Natural Ventilation Augmented Cooling (NVAC) greenhouse. *Biosystems Engineering* 174: 173-189.

Khaoua, S.O., Bournet, P.E., Migeon, C., Boulard, T., Chasseriaux, G. 2006. Analysis of greenhouse ventilation efficiency based on computational fluid dynamics. *Biosystems Engineering* 95: 83-98.

Perén, J.I., Van hooff, T., Leite, B.C.C., Blocken, B. 2016. CFD simulation of wind-driven upward cross ventilation and its enhancement in long buildings: Impact of single-span versus double-span leeward sawtooth roof and

opening ratio. *Building and Environment* 96: 142-156.

Piscia, D., Muñoz, P., Panadès, C., Montero, J.I. 2015. A method of coupling CFD and energy balance simulations to study humidity control in unheated greenhouses. *Computers and Electronics in Agriculture* 115: 129-141.

Reynafarje, X., Villagrán, E.A., Bojacá, C.R., Gil, R., Schrevens, E. 2020. Simulation and validation of the airflow inside a naturally ventilated greenhouse designed for tropical conditions. *Acta Horticulturae* 1271: 55-62.

Rodríguez-Leyton, M. 2019. Desafíos para el consumo de frutas y verduras. *Revista de la Facultad de Medicina Humana* 19: 105-112.

Román-Roldán, N.I., López-Ortiz, A., Ituna-Yudonago, J.F., García-Valladares, O., Pilatowsky-Figueroa, I. 2019. Computational fluid dynamics analysis of heat transfer in a greenhouse solar dryer "chapel-type" coupled to an air solar heating system. *Energy Science & Engineering 7*:1123-1139.

Saberian, A., Sajadiye, S.M. 2019. The effect of dynamic solar heat load on the greenhouse microclimate using CFD simulation. *Renewable Energy*, 138, 722-737.

Senhaji, A., Mouqallid, M., Majdoubi, H. 2019. CFD assisted study of multi-chapels greenhouse vents openings effect on inside airflow circulation and microclimate patterns. *Open Journal of Fluid Dynamics* 9: 119-139.

Taki, M., Ajabshirchi, Y., Ranjbar, S.F., Rohani, A., Matloobi, M. 2016. Modeling and experimental validation of heat transfer and energy consumption in an innovative greenhouse structure. *Information Processing in Agriculture 3:* 157-174.

Teitel, M., Montero, J.I., Baeza, E.J. 2012. Greenhouse design: concepts and trends. *Acta Horticulturae* 952: 605-620.

Toghraie, D., Abdollah, M. D., Pourfattah, F., Akbari, O. A., Ruhanl, B. 2018. Numerical investigation of flow and heat transfer characteristics in smooth, sinusoidal and zigzag-shaped microchannel with and without nanofluid. *Journal of Thermal Analysis and Calorimetry* 131: 1757-1766.

Villagrán, E., Bojacá, C. 2020. Analysis of the microclimatic behavior of a greenhouse used to produce carnation (Dianthus caryophyllus L.). *Ornamental Horticulture* 26: 109–204.

Villagrán, E., Ramirez, R., Rodriguez, A., Pacheco, R.L., Jaramillo, J. 2020. Simulation of the Thermal and Aerodynamic Behavior of an Established Screenhouse under Warm Tropical Climate Conditions: A Numerical Approach. *International journal of sustainable development and planning* 15: 487-499.

Villagrán, E. A., Romero, E. J. B., Bojacá, C. R. 2019. Transient CFD analysis of the natural ventilation of three types of greenhouses used for agricultural production in a tropical mountain climate. *Biosystems Engineering 188*: 288-304.

Villagrán Munar, E.A., Bojacá Aldana, C.R. 2019. Simulación del microclima en un invernadero usado para la producción de rosas bajo condiciones de clima intertropical. *Chilean journal of agricultural & animal sciences* 35: 137-150.

Conflict of Interest Statement: The authors declare that the research was conducted in the absence of any commercial or financial relationships that could be construed as a potential conflict of interest.